Highly Sensitive Electrochemical Sensor Based on rGO/Fe₃O₄ Composite as Electrocatalyst for Clenbuterol Detection in Doping Analysis

Yu Sun[1], Ting Wang[2], Sheng Chen[3,*], Xiao Wang [4], Lino C. Reynoso[5]

[1] Basic Science Department, Wuchang Shouyi University, Wuhan Hubei, 430064, China
[2] College of Physical Education, Chengdu University, Chengdu, 610106, China
[3] College of Physical Education, Southwest University, Chongqing, 400715, China
[4] Tennis Teaching and Research Office, Physical Education And Training of Tired Department, Chengdu Sport University, Chengdu, 610000, China
[5] Graduate School, Emilio Aguinaldo College, Manila 1007, Philippines
*E-mail: shengchen0715@163.com

Clenbuterol has anabolic effects as a doping agent and is banned by the World Anti-Doping Agency for use by athletes. If an athlete consumes pork with clenbuterol residues, it may cause a positive urine test result, which will seriously affect the athletic career. In this work, an electrochemical sensor for the detection of clenbuterol was proposed. Two reduced graphene oxide/Fe₃O₄ (rGO/Fe₃O₄) nanocomposites were prepared by solvent thermal and hydrothermal methods. Different rGO/Fe₃O₄ were characterized and compared with FT-IR, XRD, SEM, and Zeta potential meters. The results show that the rGO/Fe₃O₄ prepared by different methods vary in surface functional groups, Fe₃O₄ crystal structures and particle sizes, surface morphology and surface charge. The electrode was modified with rGO/Fe₃O₄ and the detection performance of the sensor for clenbuterol was investigated. Under optimal conditions, the electrochemical sensor could linearly detect clenbuterol from 1 µM - 128 µM with a detection limit of 120 nM. In addition, this electrochemical sensor has been successfully used for the detection of clenbuterol in swine urine.

1. INTRODUCTION

Clenbuterol is a synthetic β₂-adrenoceptor agonist. Its pharmacological effects are to relax bronchial smooth muscle, increase lung volume, reduce airway resistance, enhance bronchial cilia movement and promote sputum expulsion. It is commonly used in clinical practice to prevent and treat asthma, emphysema and other respiratory diseases [1–5]. In addition, clenbuterol also has anabolic

effects, thus as a stimulant, the drug is an anabolic agent prohibited for use by athletes by the World Anti-Doping Agency (WADA). In recent years, clenbuterol has been illegally used in the feeding of live pigs, since its anabolic effects can promote muscle growth and reduce fat mass. However, it can remain in the muscle tissue and internal organs of the animals being fed. Clenbuterol is relatively stable in chemical structure and is not easily broken down in the body [6,7]. Only half of the residue can be destroyed when meat containing the drug is fried in oil at 126°C for 5 min. Therefore, conventional cooking cannot destroy clenbuterol residues. If athletes consume pork with clenbuterol residue, it may even cause a positive urine test result, which will seriously affect their athletic career [8].

Liquid chromatography is a common method for the detection of clenbuterol residues. Due to the hydrophobic interaction between clenbuterol and the stationary phase, a number of research groups have been working on it with reversed-phase chromatography [9–12]. Chromatography is a well-established separation method based on the difference in the interaction between the mobile phase and the stationary phase, which can successfully separate the mixture. The combination of chromatography with different detection means can achieve the dual purpose of separation and detection. The routine operation of liquid chromatography is that the target sample is extracted and purified, then heated by ultrasonic dispersion of chloroauric acid and extracted with isopropyl alcohol plus ethyl acetate [13–16]. The separation is carried out on a cation exchange column, eluted with ethanol plus ammonia eluent, and detected on a high performance liquid chromatography (HPLC) column only after methanolic fixation with the mobile phase sodium dihydrogen phosphate. Finally the quantitative results are calculated by external standard method. The detection of clenbuterol by gas chromatography is complicated due to the derivatization of the product during the separation process [17–19]. The separation can be improved by modifying the separation process, such as repeating the column separation, or capillary column separation. The detection of clenbuterol by GC-MS starts with the derivatization of the polar functional groups it contains, such as light groups and amino groups, which is conventionally done by methylsilylation. This method can be summarized as the following process: a sample containing clenbuterol is dispersed in hexamethyldisilazane at 30° and clenbuterol is obtained by solid phase extraction before being detected by GC-MS analysis [20].

Electrochemical sensors have received great attention because of their superior performance such as simple operation, portability, and easy field monitoring. In this study, reduced graphene oxide-Fe_3O_4 nanocomposites were prepared. The adsorption properties of the composites were investigated and modified onto the surface of glassy carbon electrodes to prepare clenbuterol electrochemical sensors for the direct electrochemical detection of clenbuterol residues in animal metabolism.

2. EXPERIMENTAL

2.1 Materials and instruments

Graphite powder, potassium permanganate ($KMnO_4$), concentrated sulfuric acid (H2SO4), hydrogen peroxide (H_2O_2, 30%), hydrochloric acid (HCl), anhydrous ferric chloride ($FeCl_3$), sodium acetate (NaOAc), diethylene glycol monohydrate (DEG), sodium chloride (NaCl), ferric sulfate

heptahydrate (FeSO$_4$-7H$_2$O), ammonia (NH$_4$OH, purity >99%) were purchased from Biological Products Laboratory (Beijing).

The UV-Visible spectrophotometer is Shimadzu's UV-2700 model. The magnetic stirrer with thermostatic heating is DF-101S from Zhengzhou Great Wall Science and Technology Co. The FTIR spectrometer is Nicolet Nexus 470. The scanning electron microscope is Zeiss supra55, and the electrochemical workstation is CHI760E.

2.2 Preparation of graphite oxide

Graphite oxide was prepared by a modified Hummers method. The procedure is as follows: 80 mL of concentrated H$_2$SO$_4$ and 2 g of graphite powder were added to a 1000 mL flask and stirred in an ice bath. The solution was transferred to a water bath at 40°C and stirred for 1 h. Afterwards, 160 mL deionized water was added and the reaction was carried out at high temperature, and the mixed solution was stirred in a water bath at 90°C for a period of time. Finally, 480 mL of deionized water and 30 mL of 30% H$_2$O2 were added to the flask at room temperature and the solution turned bright yellow. The resulting product was washed with 5% HCl to remove metal ions and then washed with deionized water to be close to neutrality. The resulting solid was freeze-dried for 24 h and prepared for use.

2.3 Preparation of reduced graphite oxide/Fe$_3$O$_4$ nanocomposites

The rGO/Fe$_3$O$_4$ nanocomposites were synthesized by solvothermal and hydrothermal methods, respectively and they were named as rGO/Fe$_3$O$_4$-1 and rGO/Fe$_3$O$_4$-2, respectively. In addition, the mass ratio of graphite oxide and iron salt was controlled at about 1:5 during the preparation of the composites.

Solvothermal method: 7 mg of graphite oxide was weighed and dispersed into 10 mL of DEG and sonicated for 3 h to form GO dispersion A, after which 34 mg of FeCl$_3$ and 63 mg of NaOAc were weighed and sonicated into 24 mL of DEG to form a clear solution B. The mixture of A and B was sonicated for 1 h. Finally, the mixture was added to a high-temperature autoclave and placed in an oven at 190°C for 4 h. After the reaction, the reactor was cooled naturally at room temperature and the products were washed with ethanol and deionized water, respectively. The product was dried in a vacuum oven at 60°C for 12 h.

Hydrothermal method: 0.1 g of graphite oxide was weighed and added to 40 mL of deionized water, which was ultrasonically dispersed for 1 h to form a stable GO suspension. 0.556 g FeSO$_4$.7H$_2$O was weighed in a beaker, and10 mL of deionized water was added to dissolve it. Afterwards, it was added to the GO suspension after dissolution, and 5 mL of 0.1 M NaOH was added to the mixture at the same time. The mixture was stirred at room temperature for 1 h. Finally, the mixture was transferred to the reactor and reacted at 180°C for 8 h. After the reactor was cooled naturally at room temperature, the products were washed several times with ethanol and deionized water, and dried under vacuum at 60°C for 12 h.

2.4 Adsorption kinetics of metal ions and adsorption isotherm experiments

In order to study the adsorption equilibrium time and adsorption mechanism of rGO/Fe_3O_4, adsorption kinetics experiment was conducted. 10 mg of the two rGO/Fe_3O_4 were weighed separately and added to a centrifuge tube containing 20 mL of a known concentration of metal ion solution, and then the tube was placed on a water bath shaker for extraction. The centrifuge tubes were removed at different time intervals (5, 10, 20, 30, 40, 60, 80, 100 min), the complexes were separated by magnets, and the supernatant was collected. After filtration through a membrane, the concentration of metal ions in the supernatant was determined on an atomic spectrophotometer.

2.5 Electrochemical detection of clenbuterol

Cyclic voltammetry (CV) and differential pulse voltammetry (DPV) were adopted for electrochemical characterization and measurement. The CV conditions were as follows: scanning voltage: 0.2 V~0.7 V, and sweep speed: 50 mV/s. The cyclic voltammograms of the bare electrode and two rGO/Fe_3O_4 composite modified glassy carbon electrodes (GCE) were obtained. A Pt wire and a Ag/AgCl (3M KCl) were applied as counter electrode and reference electrode, respectively.

3. RESULTS AND DISCUSSION

Figure 1 shows the IR spectra of graphite oxide, rGO/Fe_3O_4-1 and rGO/Fe_3O_4-2. Graphite oxide has a strong absorption peak at $3410 \, cm^{-1}$, which belongs to the O-H stretching vibration. The absorption peaks at $1725 \, cm^{-1}$ and $1622 \, cm^{-1}$ belong to the C=O and C=C stretching vibrations, respectively. The peaks of C-O stretching vibration in epoxy group and alkoxy group are at $1226 \, cm^{-1}$ and $1055 \, cm^{-1}$, respectively. Moreover, it can be seen that an absorption band belongs to the COO-symmetric vibration at $1410 \, cm^{-1}$ [21,22]. The appearance of these oxygen-containing groups indicates that the graphite powder has been successfully oxidized to graphite oxide. In rGO/Fe_3O_4-1 and rGO/Fe_3O_4-2, the absorption peaks at $1725 \, cm^{-1}$ and $1410 \, cm^{-1}$ disappear, and the peak intensity of the absorption spectrum band near $1622 \, cm^{-1}$ decreases significantly, which proves that the graphite oxide has been reduced. In addition, a new absorption peak appears near $1582 \, cm^{-1}$, which may be the skeleton vibration of the graphene sheet [23–25]. The strong absorption peak at $580 \, cm^{-1}$ is the vibration of Fe-O in Fe_3O_4, indicating that the Fe_3O_4 nanoparticles have been successfully modified on the reduced graphene oxide sheet. It is noteworthy that the absorption intensity of the absorption bands at $1630 \, cm^{-1}$, $1580 \, cm^{-1}$ and $1076 \, cm^{-1}$ in rGO/Fe_3O_4-1 is larger than that of the peak in rGO/Fe_3O_4-2, the reason for which may be the presence of more oxygen-containing groups on the surface of rGO/Fe_3O_4-1 [26–28]. Furthermore, the weaker vibrational intensity of Fe-O in rGO/Fe_3O_4-1 compared with rGO/Fe_3O_4-2 indicates the smaller loading of Fe_3O_4 nanoparticles in rGO/Fe_3O_4-1.
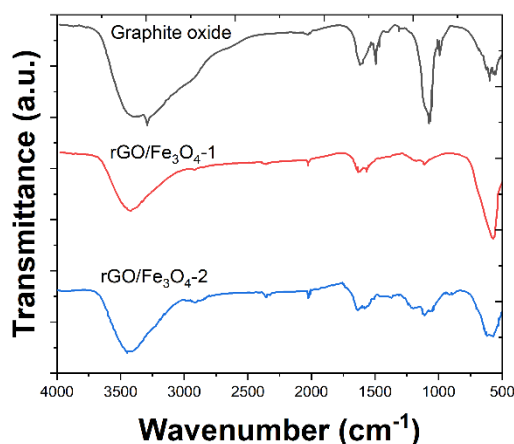
Figure 1. Infrared spectra of graphite oxide, rGO/Fe$_3$O$_4$-1 and rGO/Fe$_3$O$_4$-2.

Figure 2 shows the XRD patterns of graphite oxide, rGO/Fe$_3$O$_4$-1 and rGO/Fe$_3$O$_4$-2. In the XRD pattern of graphite oxide, there is a sharp peak belonging to graphite oxide at the diffraction angle 2θ=10.8°, which proves the successful preparation of graphite oxide. In the XRD plots of both rGO/Fe$_3$O$_4$-1and rGO/Fe$_3$O$_4$-2, six characteristic diffraction peaks consistent with the Fe$_3$O$_4$ standard card (JCPDS No. 19-0629) appear, and the diffraction angles 2θ of these peaks are 30.2°, 35.6°, 43.3°, 57.3°, 62.8°, 74.9°, corresponding to (220), (311), (400), (511), (440), and (533) crystal planes of Fe$_3$O$_4$ nanoparticles [29]. In addition, a broad peak appears at the diffraction angle of 2θ = 24.3°, which is the reduced graphene oxide (002) crystallographic plane diffraction peak. The appearance of these peaks confirms that the nanocomposites have been prepared successfully, and the results are consistent with FTIR.
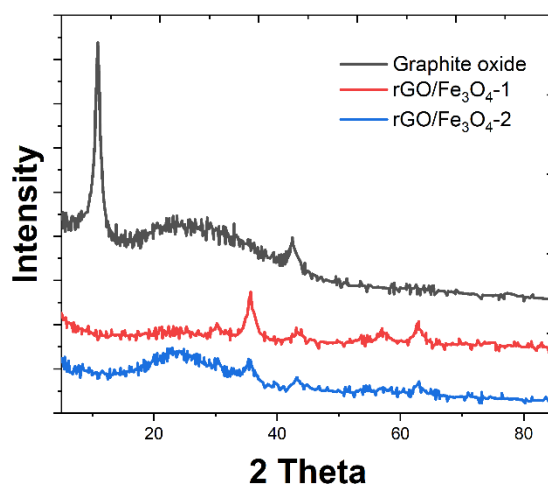

Figure 2. XRD patterns of graphite oxide, rGO/Fe$_3$O$_4$-1 and rGO/Fe$_3$O$_4$-2.

Figure 3 shows the SEM images of rGO/Fe$_3$O$_4$-1 and rGO/Fe$_3$O$_4$-2. It can be noted from the figure that rGO/Fe$_3$O$_4$ has a three-dimensional spatial morphological feature. The small size Fe$_3$O$_4$ nanoparticles (the small bright spots in the figure) are uniformly and densely loaded on the rGO layer sheet with a folded structure [30]. Moreover, it is obvious that the particle size of Fe$_3$O$_4$ nanoparticles loaded on rGO/Fe$_3$O$_4$-1 is smaller than that of Fe$_3$O$_4$ nanoparticles on rGO/Fe$_3$O$_4$-2.
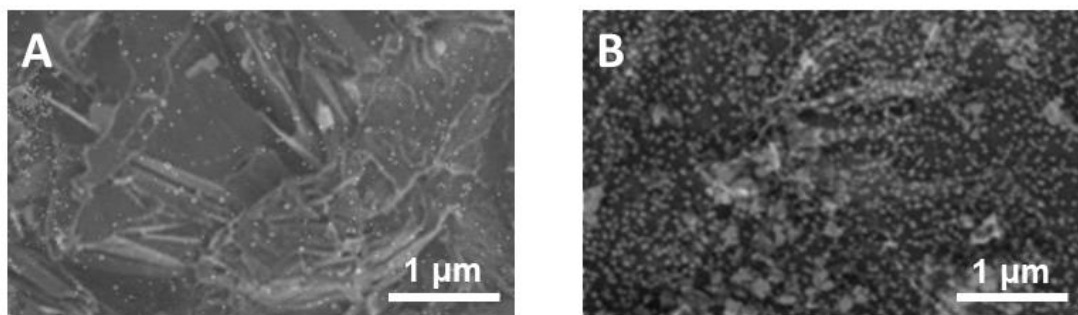

Figure 3. SEM images of (A) rGO/Fe$_3$O$_4$-1 and (B) rGO/Fe$_3$O$_4$-2.

Zeta potential is widely adopted to characterize the charge level on the adsorbent surface. rGO/Fe$_3$O$_4$-1 and rGO/Fe$_3$O$_4$-2 have a zeta potential of -18.30 mV and -4.03 mV, respectively, indicating that their surfaces are negatively charged, which is favorable for the adsorption of metal cations.
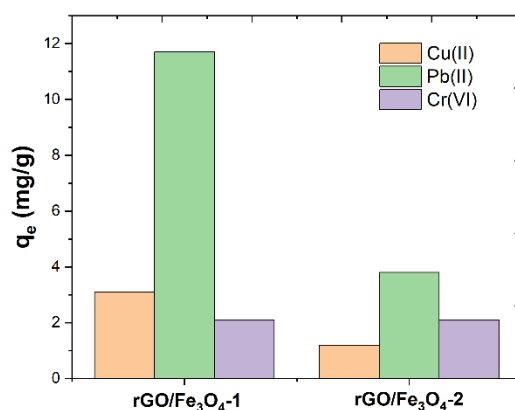

Figure 4. Adsorption ability of rGO/Fe$_3$O$_4$-1 and rGO/Fe$_3$O$_4$-2 for the removal of metal ions (temperature 25°C, pH=7).

Figure 4 compares the extraction ability of rGO/Fe$_3$O$_4$-1 and rGO/Fe$_3$O$_4$-2 for Cu(II), Pb(II) and Cr(VI). It is apparent that rGO/Fe$_3$O$_4$-1 has a strong extraction ability for Pb(II), while rGO/Fe$_3$O$_4$-2 has the maximum extraction for Cr(VI). rGO/Fe$_3$O$_4$-1 and rGO /Fe$_3$O$_4$-2 have similar magnitude of extraction for Cu(II). rGO/Fe$_3$O$_4$-1 and rGO/Fe$_3$O$_4$-2 have similar order of extraction ability for the three

ions: Pb(II)>Cu(II)>Cr(VI). rGO/Fe$_3$O$_4$-1 and rGO/Fe$_3$O$_4$-2 have similar order of extraction ability for the three ions. The adsorption behavior of different metal ions on the surface of rGO/Fe$_3$O$_4$ materials is firstly determined by the charges carried on the surface of the complexes and secondly related to the ionic radii of the metal ions [31,32]. In addition, the specific surface area of the different complex surfaces and the coordination ability of the surface groups of the complexes to the metal ions should be considered [33]. In order to further understand the adsorption behavior of metal ions on the complex surfaces, their adsorption kinetics and adsorption isotherms were investigated.

To further study the differences in the adsorption performance of rGO/Fe$_3$O$_4$ prepared by different methods, which is represented by metal ions, the effect of adsorption time on the removal of metal ions by different complexes was analyzed in Figure 5. It can be seen from the figure that the adsorption equilibrium time are 60 min and 100 min for Cr(VI) and Cu(II), respectively, while the adsorption equilibrium time is longer than 180 min for Pb(II). The possible reason is the different hydrated ionic radii of ions, which increase sequentially for Cr(VI), Cu(II), and Pb(II).
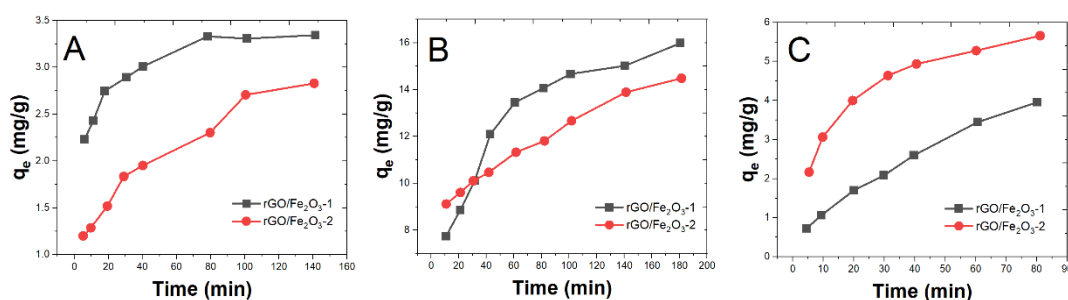

Figure 5. Kinetic adsorption data plots for (A) Cu(II), (B) Pb(II) and (C) Cr(VI) on rGO/Fe$_3$O$_4$-1 and rGO/Fe$_3$O$_4$-2: plot of adsorption capacity qt vs. time t.
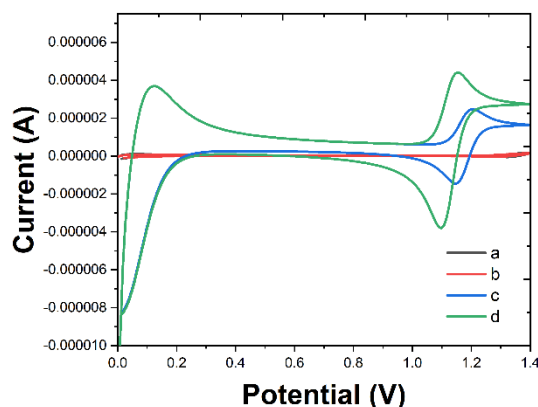
Figure 6. Cyclic voltammograms of (a) rGO/Fe$_3$O$_4$-1 and (b) rGO/Fe$_3$O$_4$-2 modified electrode in 0.1 M HClO$_4$; and (c) rGO/Fe$_3$O$_4$-1 and (d) rGO/Fe$_3$O$_4$-2 modified electrode in 0.1 M HClO$_4$ containing 0.01 mM clenbuterol.

Figure 6 compares the cyclic voltammograms of the rGO/Fe$_3$O$_4$-1 and rGO/Fe$_3$O$_4$-2 modified electrodes in 0.1 M HClO$_4$ with and without clenbuterol. The background currents can be observed from

Curve a and Curve b. As seen from the Curve c and Curve d, the peak current increases when 0.01 mM clenbuterol is added, indicating that the catalytic effect of rGO/Fe$_3$O$_4$ on clenbuterol is significant. Meanwhile, through comparing rGO/Fe$_3$O$_4$-1 and rGO/Fe$_3$O$_4$-2, it can be found that rGO/Fe$_3$O$_4$-2 has a better detection effect. The excellent electrocatalytic performance of the rGO/Fe$_3$O$_4$ can be ascribed to two reasons. Firstly, the rGO serves as an excellent platform for loading Fe$_3$O$_4$ nanoparticles, significantly enhancing the surface area of Fe$_3$O$_4$ and consequently preventing the aggregation [34,35]. The fully exposure of the Fe$_3$O$_4$ surface provided the electrocatalytic sites for clenbuterol to take electrochemical reaction. Secondly, the absorption of the rGO with clenbuterol can also concentrated the local analyte and give a superior sensing signal [36,37].

   In this study, the electrochemical behavior of clenbuterol in HClO$_4$, NaOH, H$_2$SO$_4$, PBS and NaAc-HAc (Figure 7) was examined. The results show that the response current is enhanced with increasing acidity, while essentially no response shows in neutral and basic solutions. 0.01 mM clenbuterol in HClO$_4$ shows the largest peak current and the best peak shape for the differential pulse. Moreover, the concentration of HClO$_4$ was optimized. The peak current of clenbuterol was the largest when the concentration of HClO$_4$ was 0.1 M. Therefore, 0.1 M HClO$_4$ was chosen as the test substrate for this clenbuterol electrochemical sensor.
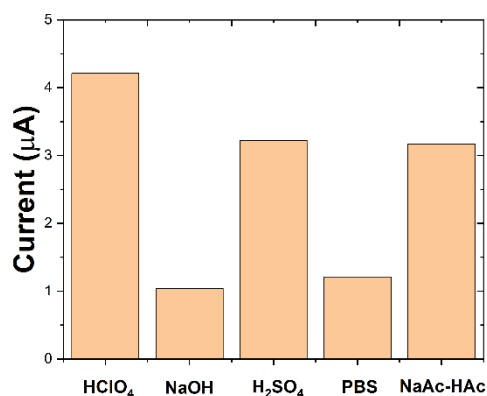

Figure 7. Current responses of the rGO/Fe$_3$O$_4$-2 modified electrode toward 0.01 mM clenbuterol under HClO$_4$, NaOH, H$_2$SO$_4$, PBS and NaAc -HAc.

   The effect of the enrichment potential on the peak current of this electrochemical sensor was investigated in 0.1 M HClO$_4$ containing 0.01 mM clenbuterol. The peak current reached the maximum at -0.1 V between -0.3 and + 0.30 V. Therefore, -0.10 V was adopted as the enrichment potential in this experiment. The peak current of clenbuterol increased with the enrichment time from 50 to 130 s, but the current leveled off after 90s. Therefore, 90s was adopted as the best enrichment time for this experiment.

   The performance of the rGO/Fe$_3$O$_4$-2 modified electrode was investigated under the optimal experimental conditions for the detection of clenbuterol. Figure 8 presents the differential pulse voltammetry (DPV) curves obtained by incubating the sensor electrode in different concentrations of

clenbuterol. When the concentration of the clenbuterol increases, the peak current also increases gradually, and at the concentration of the clenbuterol solution of 128 µM, the difference of the peak current of DPV maintains a good linear relationship with the logarithm of the clenbuterol concentration, and the detection limit is 120 nM (S/N=3).

Table 1 presents the comparison between the sensing properties of Pt-Pd/Au with reported glucose sensors in literature. As shown in Table 1, the sensitivity and detection limit of Pt-Pd/Au is better than other glucose sensors which indicating more stability and more active electrochemical sites on nanostructured Pt-Pd surface.
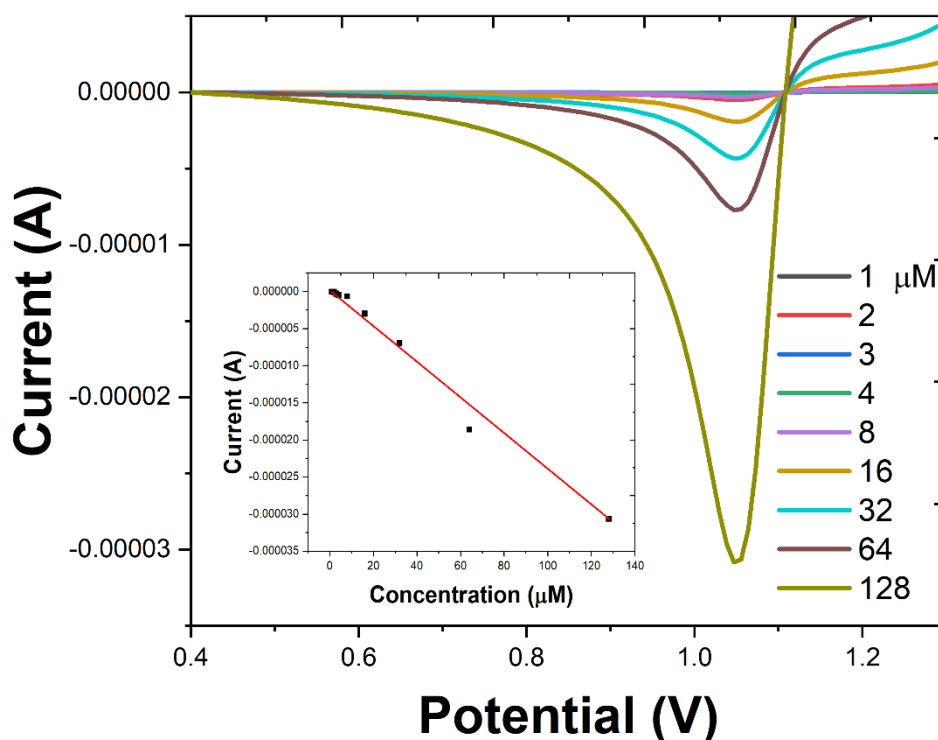

Figure 8. DPV of rGO/Fe$_3$O$_4$-2 modified electrode towards clenbuterol from 0.2 µM to 50 mM. Inset: Calibration curve of current against the logarithm of the clenbuterol concentration.

Table 1. Comparison between the sensing properties of rGO/Fe$_3$O$_4$-2 modified electrode with reported clenbuterol sensors in literatures.

Sensor	Linear range	Limit of detection	Ref.
Nafion–Au/GCE	0.8 µM -10 µM	0.1 µM	[38]
MoS$_2$-Au-PEI-hemin	1 µM -40 µM	0.15 µM	[39]
Cl/MIP/Au	2 µM -100 µM	0.031µM	[40]
KVB-Nf (IP)/FCE	0.95µM -14.31 µM	0.75µM	[41]
rGO/Fe$_3$O$_4$-2 modified electrode	1 µM - 128 µM	120 nM	This work

The electrochemical sensor was applied in testing the recovery of clenbuterol in untreated pig urine (Table 2) to examine its usefulness.

Table 2. Recovery of proposed electrochemical sensor in pig urine sample.

Sample	Added (μM)	Found (μM)	Recovery (%)
1	1.00	0.97	97.00
2	5.00	5.06	101.20
3	10.00	10.17	101.70

4. CONCLUSION

rGO/Fe_3O_4 is a novel magnetic nanocomposite that combines the excellent properties of graphene and Fe_3O_4 nanoparticles with good dispersion, huge specific surface area, super magnetic properties and excellent extraction ability. In this work, two rGO/Fe_3O_4 composites were synthesized and characterized and it was found that the rGO/Fe_3O_4--2 synthesized by hydrothermal method is more suitable for electrode modification and for the highly sensitive detection of clenbuterol. Under optimal conditions, the electrochemical sensor can provide linear detection of 1 μM - 128 μM clenbuterol with a detection limit of 120 nM.

References

1. T. Peng, J. Wang, S. Zhao, Y. Zeng, P. Zheng, D. Liang, G.M. Mari, H. Jiang, *Anal. Chim. Acta*, 1040 (2018) 143–149.
2. T. Simon, M. Shellaiah, P. Steffi, K.W. Sun, F.-H. Ko, *Anal. Chim. Acta*, 1023 (2018) 96–104.
3. J. Zhou, Y. Zheng, J. Zhang, H. Karimi-Maleh, Y. Xu, Q. Zhou, L. Fu, W. Wu, *Anal. Lett.*, 53 (2020) 2517–2528.
4. J. Liu, T. Yang, J. Xu, Y. Sun, *Front. Chem.*, 9 (2021) 488.
5. H. Karimi-Maleh, Y. Orooji, F. Karimi, M. Alizadeh, M. Baghayeri, J. Rouhi, S. Tajik, H. Beitollahi, S. Agarwal, V.K. Gupta, *Biosens. Bioelectron.* (2021) 113252.
6. Y. Chen, Z. Huang, S. Hu, G. Zhang, J. Peng, J. Xia, W. Lai, *Anal. Biochem.*, 577 (2019) 45–51.
7. H. Karimi-Maleh, M. Alizadeh, Y. Orooji, F. Karimi, M. Baghayeri, J. Rouhi, S. Tajik, H. Beitollahi, S. Agarwal, V.K. Gupta, S. Rajendran, S. Rostamnia, L. Fu, F. Saberi-Movahed, S. Malekmohammadi, *Ind. Eng. Chem. Res.*, 60 (2021) 816–823.
8. X. Jin, G. Fang, M. Pan, Y. Yang, X. Bai, S. Wang, *Biosens. Bioelectron.*, 102 (2018) 357–364.
9. Y. Cong, H. Dong, X. Wei, L. Zhang, J. Bai, J. Wu, J.X. Huang, Z. Gao, H. Ueda, J. Dong, *Ecotoxicol. Environ. Saf.*, 182 (2019) 109473.
10. Q. Huang, T. Bu, W. Zhang, L. Yan, M. Zhang, Q. Yang, L. Huang, B. Yang, N. Hu, Y. Suo, J. Wang, D. Zhang, *Food Chem.*, 262 (2018) 48–55.
11. Y. Xu, Y. Lu, P. Zhang, Y. Wang, Y. Zheng, L. Fu, H. Zhang, C.-T. Lin, A. Yu, *Bioelectrochemistry*, 133 (2020) 107455.
12. L. Fu, Y. Zheng, P. Zhang, H. Zhang, M. Wu, H. Zhang, A. Wang, W. Su, F. Chen, J. Yu, W. Cai, C.-T. Lin, *Bioelectrochemistry*, 129 (2019) 199–205.
13. L. Ma, A. Nilghaz, J.R. Choi, X. Liu, X. Lu, *Food Chem.*, 246 (2018) 437–441.

14. R. Duan, X. Fang, D. Wang, *Front. Chem.*, 9 (2021) 361.
15. Z. Xu, M. Peng, Z. Zhang, H. Zeng, R. Shi, X. Ma, L. Wang, B. Liao, *Front. Chem.*, 9 (2021) 683.
16. H. Karimi-Maleh, A. Ayati, R. Davoodi, B. Tanhaei, F. Karimi, S. Malekmohammadi, Y. Orooji, L. Fu, M. Sillanpää, *J. Clean. Prod.*, 291 (2021) 125880.
17. N. Duan, S. Qi, Y. Guo, W. Xu, S. Wu, Z. Wang, *LWT*, 134 (2020) 110017.
18. Z. Wang, J. Jing, Y. Ren, Y. Guo, N. Tao, Q. Zhou, H. Zhang, Y. Ma, Y. Wang, *Mater. Lett.*, 234 (2019) 212–215.
19. S. Wei, X. Chen, X. Zhang, L. Chen, *Front. Chem.*, 9 (2021) 697.
20. Z. Ma, Q. Wang, N. Gao, H. Li, *Microchem. J.*, 157 (2020) 104911.
21. B. Zhang, X. Fan, D. Zhao, *Polymers*, 11 (2019).
22. H. Karimi-Maleh, F. Karimi, L. Fu, A.L. Sanati, M. Alizadeh, C. Karaman, Y. Orooji, *J. Hazard. Mater.*, 423 (2022) 127058.
23. Z. Wu, J. Liu, M. Liang, H. Zheng, C. Zhu, Y. Wang, *Front. Chem.*, 9 (2021) 208.
24. M. Zhang, B. Pan, Y. Wang, X. Du, L. Fu, Y. Zheng, F. Chen, W. Wu, Q. Zhou, S. Ding, *ChemistrySelect*, 5 (2020) 5035–5040.
25. L. Fu, Y. Zheng, P. Zhang, H. Zhang, Y. Xu, J. Zhou, H. Zhang, H. Karimi-Maleh, G. Lai, S. Zhao, W. Su, J. Yu, C.-T. Lin, *Biosens. Bioelectron.*, 159 (2020) 112212.
26. Y. Zheng, H. Zhang, L. Fu, *Inorg. Nano-Met. Chem.*, 48 (2018) 449–453.
27. W. Long, Y. Xie, H. Shi, J. Ying, J. Yang, Y. Huang, H. Zhang, L. Fu, *Fuller. Nanotub. Carbon Nanostructures*, 26 (2018) 856–862.
28. N.A.A. Talib, F. Salam, Y. Sulaiman, *Sensors*, 18 (2018).
29. L. Wang, H. Zhang, L. Su, X. Yao, Z. Wang, M. Zhao, J. Sun, J. Wang, D. Zhang, *Sens. Actuators B Chem.*, 331 (2021) 129443.
30. Y. Zheng, Y. Huang, H. Shi, L. Fu, *Inorg. Nano-Met. Chem.*, 49 (2019) 277–282.
31. L. Zhang, Q. Wang, Y. Qi, L. Li, S. Wang, X. Wang, *Sens. Actuators B Chem.*, 288 (2019) 347–355.
32. B. Zhao, Q. Huang, L. Dou, T. Bu, K. Chen, Q. Yang, L. Yan, J. Wang, D. Zhang, *Sens. Actuators B Chem.*, 275 (2018) 223–229.
33. J. Li, S. Zhang, L. Zhang, Y. Zhang, H. Zhang, C. Zhang, X. Xuan, M. Wang, J. Zhang, Y. Yuan, *Front. Chem.*, 9 (2021) 339.
34. D. Wu, Y. Li, Y. Zhang, P. Wang, Q. Wei, B. Du, *Electrochimica Acta*, 116 (2014) 244–249.
35. L. Cai, B. Hou, Y. Shang, L. Xu, B. Zhou, X. Jiang, X. Jiang, *Chem. Phys. Lett.*, 736 (2019) 136797.
36. Z. Xu, X. Fan, Q. Ma, B. Tang, Z. Lu, J. Zhang, G. Mo, J. Ye, J. Ye, *Mater. Chem. Phys.*, 238 (2019) 121877.
37. Y. Poo-arporn, S. Pakapongpan, N. Chanlek, R.P. Poo-arporn, *Sens. Actuators B Chem.*, 284 (2019) 164–171.
38. L. Liu, H. Pan, M. Du, W. Xie, J. Wang, *Electrochimica Acta*, 55 (2010) 7240–7245.
39. Y. Yang, H. Zhang, C. Huang, D. Yang, N. Jia, *Biosens. Bioelectron.*, 89 (2017) 461–467.
40. L. Liu, C. Long, S. Wei, Y. Sun, *Int J Electrochem Sci*, 16 (2021) 210411.
41. K. Zhang, Y. Ge, S. He, F. Ge, Q. Huang, Z. Huang, X. Wang, Y. Wen, B. Wang, *Int J Electrochem Sci*, 15 (2020) 7326–7336.